




Near-infrared and green light emission spectroscopic characteristics of Er³⁺ doped alumina–phosphate glasses

Vinod Hegde¹ · K. R. Vighnesh² · Sudha D. Kamath² · C. S. Dwaraka Viswanath³ · Aljawhara H. Almuqrin⁴ · M. I. Sayyed^{5,6} · Jagannath Gangareddy^{7,8} · R. Rajaramakrishna⁹ · K. Keshavamurthy¹⁰ 

Received: 5 February 2024 / Accepted: 17 April 2024

© The Author(s), under exclusive licence to Springer-Verlag GmbH Germany, part of Springer Nature 2024

Abstract

Trivalent erbium ions doped (48–*x*) AlPO₄ + 15K₂O + 12MgF + 20Na₂O + 5NaF + *x*Er₂O₃ glass samples have been prepared utilizing the melt-quench process and studied to understand the efficacy of Er³⁺ ions content on physical, structural and luminescence attributes of host glass. The functional groups of the glass structure such as metaphosphate, orthophosphate and pyrophosphate have been elucidated through Fourier Transform Infrared (FTIR) spectroscopic investigation. The least-square approach was used to calculate the Judd–Ofelt parameter from the oscillator strength of the Er³⁺ ion transitions. The luminescence emission data captured in the visible and near-infrared (NIR) province using 380 and 980 nm excitation wavelengths. The up-conversion (recorded at the excitation at 980 nm) of 0.5 Er glass exhibited emission at 664, 550 and 488 nm wavelengths. The decay plots of the studied glass specimens were measured at 980 nm excitation. The McCumber (MC) theory has been implemented to calculate the gain coefficient of the 0.5 Er glass and flat gain curve was drawn for S-band, C-band and L-band. The attributes for optical amplification were ascertained, including the quality factor (0.85), branching ratio (1), stimulated emission cross-section (1.3 × 10⁻²⁰ cm²), gain bandwidth (1.26 × 10⁻²⁵ cm³) and optical gain (0.394 × 10⁻²³ cm² s) for 0.5 Er glass. The yellowish green light emission ability of the 0.5 Er glass after 980 nm excitation evident through CIE co-ordinates position (x 0.36, y 0.58) at 1931 CIE chromaticity diagram. The spectroscopic and luminescence results endorse that the alumino–phosphate glass specimens loaded with 0.5 mol% of Er₂O₃ are beneficial for NIR and green light emission applications.

Keywords Fluorophosphate glasses · Trivalent erbium ions · Optoelectronic applications · Near-infrared and green emission · Spectroscopic characteristics

✉ Sudha D. Kamath
sudhakamath6@gmail.com

✉ K. Keshavamurthy
keshav.m85@gmail.com

¹ Department of Physics, Manipal Institute of Technology Bengaluru, Manipal Academy of Higher Education, Manipal, Karnataka 576104, India

² Glass Processing Lab, Department of Physics, Manipal Institute of Technology, Manipal Academy of Higher Education, Manipal, Karnataka 576104, India

³ Department of Science and Humanities, Mother Theresa Institute of Engineering and Technology, Palamaner, Chittoor 517408, India

⁴ Department of Physics, College of Science, Princess Nourah Bint Abdulrahman University, P.O. Box 84428, 11671 Riyadh, Saudi Arabia

⁵ Department of Physics, Faculty of Science, Isra University, Amman, Jordan

⁶ Renewable Energy and Environmental Technology Center, University of Tabuk, Tabuk 47913, Saudi Arabia

⁷ Department of Physics, School of Engineering, Presidency University, Itgalpur, Rajanakunte, Yelahanka, Bengaluru, Karnataka 560064, India

⁸ Specialty Glass Division, CSIR–Central Glass and Ceramic Research Institute (CSIR–CGCRI), 196, Raja S C Mullick Road, Kolkata, West Bengal 700032, India

⁹ Siberian Federal University, Svobodny Prospect 79, Krasnoyarsk, Russia 660041

¹⁰ Department of Physics, Dayananda Sagar College of Engineering, Bengaluru, Karnataka 560078, India

1 Introduction

In modern days, optical materials have been taken into lot of research for light production and as a wavelength converter for photonics and optoelectronic devices. The luminescent ions doped glasses and crystals were considered as primary hosts for technological applications such as optical amplifier, solid-state lasers, fibre optic laser, wave guide amplifier, sensors and white light emitting diodes (WLEDs) [1–4]. Among the light emitting species, for aforementioned purposes, the rare earth (RE) ions used to dope into the glasses and polycrystalline materials for long-lasting ability to produce electromagnetic radiations upon suitable excitations. The doped glass also considered for solar energy concentrators to enhance solar cell efficiency [5].

In particular, the trivalent erbium (Er^{3+}) ions doped glasses were prime materials of research because of their unique spectral emission attributes in the visible to near-infrared (NIR) spectral span [6]. The Er^{3+} ions in its triply oxidized state are able to absorb ultra-violet–visible (UV–Vis) and NIR wavelengths and their-after shows strong luminesce due to $4f-4f$ intra-band electronic transitions [7, 8]. Among emission bands, the wide emission band around 1532 nm (C band) of Er^{3+} ions have been made worthy luminescent ions for low loss optical amplifiers [9]. The Er^{3+} doped silica glass based optical fiber amplifier has been commercialised for telecommunication on account its low loss in L band emission [10]. Nevertheless, the rise in internet usage, optical amplifier demands the materials which are capable of transmit more light channels. In this regard, the full-width half maxima (FWHM) of L band of Er^{3+} ions need to be tuned to create a lot of wavelength division multiplex channels [10, 11]. The four energy levels and high metastable lifetime of Er^{3+} ions are made former ion doped glasses as most affable to construct light gain material for visible and NIR solid-state fibre laser [9]. However, the Er^{3+} emission intensity, FWHM and stimulated emission cross-section are always intra-dependent on structural inhomogeneity of glass, bonding between Er^{3+} ions to ligand and ions concentrations [12].

Among all conventional glasses including the silicate, borate, tellurite, germanate, and phosphate, the phosphate glass samples have been considered as paradigmatic hosts for activating the Er^{3+} ions due to their thermo-chemical and mechanical robustness [13]. Additionally, the contrast to other glass systems the phosphate-based glass systems owe excellent solubility of RE ions (here, Er^{3+} ions) due to which they exhibit excellent optical properties required for optoelectronic and photonic applications [14]. Also, the phosphate glass preparation was energy efficient due to its

low melting temperature and offers high light transmission from UV to NIR optical region [1]. However, the hygroscopic decomposition nature of phosphate glasses hinders their practical usage and which has been addressed by adding alkali and alkaline oxides into phosphate glass matrix. The Er^{3+} doped in pure oxide glass is to show moderate spectral properties due to high energy phonons in the oxide glass. The emission intensity and metastable lifetime was affected due to multiphonon relaxation of Er^{3+} ions from its excited levels. Nevertheless, the presence of Er^{3+} elements in the fluoride phase of the oxyfluoride phosphate glass often enhances the emission intensity of the excited ions and spectral properties [15]. The Er^{3+} ion possesses multi excitation peaks in NIR as well as visible region. Hence, Er^{3+} ions doped in glasses have been explored for green light application via down conversion and up conversion process [16, 17]. In consideration to attain the excellent spectroscopic characteristics in NIR and green spectral provenance, in the current project, we investigate the structural and spectroscopic characteristics of varied concentrations of Er_2O_3 loaded fluorophosphate glass specimens bearing the nominal composition of $(48-x)\text{AlP}\text{O}_4 + 15\text{K}_2\text{O} + 12\text{MgF} + 20\text{Na}_2\text{O} + 5\text{NaF} + x\text{Er}_2\text{O}_3$.

2 Experimental work

The glass-forming salts for the 7.5 g batch were weighed according to the standard glass batch computation and ground well for uniform mixing. The finely powdered glass batches bearing different concentration of Er_2O_3 were filled to 7.5 g crucibles and loaded into high temperature electric furnace. The batches were melted at 1100 °C by maintaining for 45 min and later molten batches were cooled to room temperature (RT) on pre-heated stainless-steel mould. The glass specimens have been heat treated at 350 °C for 3 h to reduce the induced thermal stresses during the quenching and subsequently cooled down to RT. Further, glass specimens were subjected for polishing utilizing various grain size abberly sheets. The polished samples were utilized for optical, density and refractive index measurements.

The Rigaku mini X-Ray diffractometer with Cu–K alpha radiation has been used to analyse the glass network. The Fourier Transform Infrared (FTIR) spectrometer with Mid-IR 400–1500 cm^{-1} wavenumbers was used to scan over the samples to determine the functional units exist in the glass. The absorption data of the obtained specimens was measured with a benefit of Perkin Elmer Lambda 750-S UV-visible spectrophotometer. The Edinburg spectrofluorometer has been utilized to collect the photoluminescence spectral outcomes of glass specimens used in the current work.

3 Result and discussion

3.1 Physical attributes

The density and index of refraction measurements were carried out on glass specimens utilizing a density measurement apparatus kit and Abbe Refractometer, respectively. In density measurements, acetone was utilized as an immersion liquid and bromide naphthalene was as the contact medium in refractive index measurements. The physical attributes of

Table 1 Physical properties of Er₂O₃-loaded (48-x)AlPO₄ + 15K₂O + 12MgF + 20Na₂O + 5NaF-Er₂O₃ glasses

Er ₂ O ₃ concentration → Parameters ↓	Glass codes			
	0.1 Er	0.3 Er	0.5 Er	0.7 Er
Density (g/cm ³)	2.660	2.665	2.669	2.673
Index of refraction (n)	1.560	1.561	1.562	1.563
Molecular Weight (g/mol)	110.318	110.871	111.424	111.977
Molar volume V _m (cm ³ /mol)	41.467	41.606	41.735	41.899
Molar refraction R _m (cm ³ /mol)	13.414	13.473	13.533	13.598
Molar polarizability (×10 ⁻²⁴ cm ³)	5.320	5.344	5.368	5.393
Rare earth concentration (N _{RE}) × 10 ²⁰ (ions/cm ³)	0.145	0.4342	0.721	1.006
Inter-ionic distance (r _i) (Å)	41.048	28.494	24.058	21.534
Polaron radius (r _p) (Å)	16.539	11.481	9.694	8.677
Field strength (F) × 10 ¹⁴ /cm ²	1.0967	2.276	3.192	3.985

the glass specimens were computed using ion (Er³⁺) concentration, refractive index, and density [18]. Table 1 displays the experimental and computed physical attributes of the studied glass specimens. Glass density and index of refraction values of the glass specimens increase with the augment of Er³⁺ ions quantity in the glass network. In the current work, the Er₂O₃ added against AlPO₄ in the glass matrix and molar mass of Er₂O₃ was higher contrast to lighter to AlPO₄, thereby the density of the glass specimens improves with Er₂O₃. Table 1 shows the fact that as the quantity of Er³⁺ ions in the glass increases, the molar electron polarizability and molar volume of the glasses increase while the polaron radius and inter-ion distance decrease [19]. As Er₂O₃ is doped to AlPO₄, the glass network forms non-bridging oxygen, which is the cause of all these variations in physical attributes.

3.2 Structural properties

The structural elucidation of the glass specimens was carried out utilizing XRD and FTIR analysis. The Fig. 1a displays the XRD signatures of the studied glass specimens. The diffrused broad halo humps appeared around 25° and 45° of 2θ confirms the non-crystalline structure of the investigated glass specimens.

The Fig. 1b shows FTIR spectra of studied glasses in 600–1800 cm⁻¹ wavenumber region. It is evident from Fig. 1b that the IR vibrations of the glass network are significant in 900–1300 cm⁻¹ wavenumber range. The vibration band around 745 cm⁻¹ corresponds to the symmetric vibrations of P–O–P motifs of the Q⁽¹⁾ (pyrophosphate) phosphate chain linkages in the glass structure. While the 771 cm⁻¹ band corresponds to the stretching symmetric vibrations of oxygen atoms bridging with phosphorus

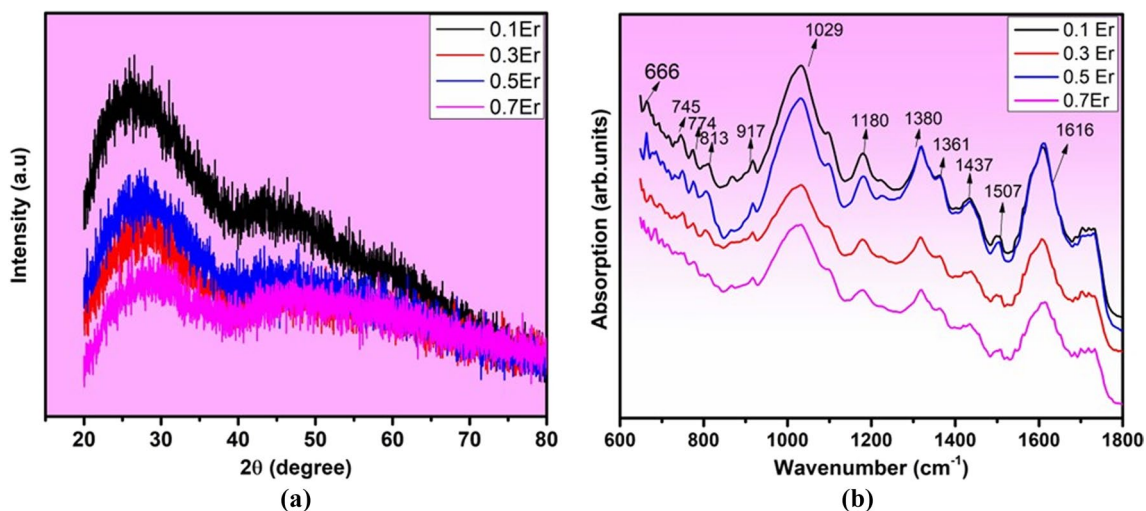


Fig. 1 XRD (a) and FTIR (b) spectra of Er₂O₃-doped (48-x)AlPO₄ + 15K₂O + 12 MgF + 20 Na₂O + 5NaF + xEr₂O₃ glasses

atoms (P–O–P) in phosphate chains. The additional weak signal around 808 cm^{-1} is owing to asymmetric stretch of non-bridging oxygens (NBOs) with phosphorus associated with $Q^{(2)}$ (metaphosphate) units [20]. The vibrational band associated with 917 cm^{-1} is connected to the occurrence of metaphosphate chained P–O bond in Q^2 (metaphosphate) linkages, occurred on account of asymmetric stretching motion of P–O–P linkages with metaphosphate chain in the glass network [21]. Thus the peak around 1085 to 1029 cm^{-1} are corresponds to vibrations of P–O symmetric stretching in PO_4 and PO_3 units from $Q^{(0)}$ (orthophosphate tetrahedra) and $Q^{(1)}$ (pyrophosphate), respectively [22]. The band at 1180 cm^{-1} is caused by the symmetric stretching of two NBOs linked with phosphorus atoms (O–P–O) in $Q^{(2)}$ (metaphosphate) units and its intensity is minimum compared with bands related to $Q^{(0)}$ and $Q^{(1)}$ units in the present phosphate network [23]. However, the IR vibration around 1317 cm^{-1} is belongs to NBOs asymmetric stretching vibrations in Q^2 (metaphosphate) motifs. The bands in higher wavenumber ($< 1350\text{ cm}^{-1}$) side are owing to vibration of P=O of Q^3 groups present in glass linkages [24]. On comparing the structural features of other non-aluminum containing fluorophosphate glasses it is clear that the, presence of glass modifier such as Al_2O_3 , etc. presently investigated glasses resulted the depolymerization of Q^2 units into Q^1 and Q^0 units in the current phosphate glass structure [25].

3.3 Optical absorption

The absorption spectral outcomes of the Er^{3+} loaded specimens were captured in the UV–Vis and NIR range. The displayed absorption spectral results in Fig. 2 showed fourteen (14) transitions caused by electronic and magnetic dipole electronic transitions within Er^{3+} ions. The ligands crystal impact on the Er^{3+} ions in the host glass is responsible for the electronic transitions within 4f energy levels. The energy difference between the ground state $^4I_{15/2}$ to $^2G_{9/2}$ excited state is 3.30 eV and for other transitions are $^4I_{15/2} \rightarrow ^4F_{3/2}$ (3.06 eV), $^4I_{15/2} \rightarrow ^4F_{5/2}$ (2.75 eV), $^4I_{15/2} \rightarrow ^4F_{7/2}$ (2.54 eV), $^4I_{15/2} \rightarrow ^2H_{11/2}$ (2.39 eV), $^4I_{15/2} \rightarrow ^4S_{3/2}$ (2.28 eV), $^4I_{15/2} \rightarrow ^4F_{9/2}$ (1.90 eV), $^4I_{15/2} \rightarrow ^4I_{9/2}$ (1.55 eV), $^4I_{15/2} \rightarrow ^4I_{11/2}$ (1.27 eV), $^4I_{15/2} \rightarrow ^4I_{13/2}$ (0.80 eV) [1]. The band intensity of the absorption transition is varied for different transition and the band at 379 nm $^4I_{15/2} \rightarrow ^2G_{9/2}$ was peaked highest in UV region. The UV and NIR provinces comprise the majority of the transitions. The characteristic NIR absorption of $^4I_{15/2} \rightarrow ^4I_{11/2}$ has appeared at 974 nm and the transition of $^4I_{15/2} \rightarrow ^4I_{13/2}$ is visible at 1534 nm . The absorption intensity of the peaks augmented with Er^{3+} ion concentration and there was no major shift in peak position. The shift of absorption band-edge of the glass specimen from lower wavelength (0.1 Er—3.50 eV) to a higher wavelength side (2 Er—3.39 eV) with respect to the doping of the Er^{3+} ion

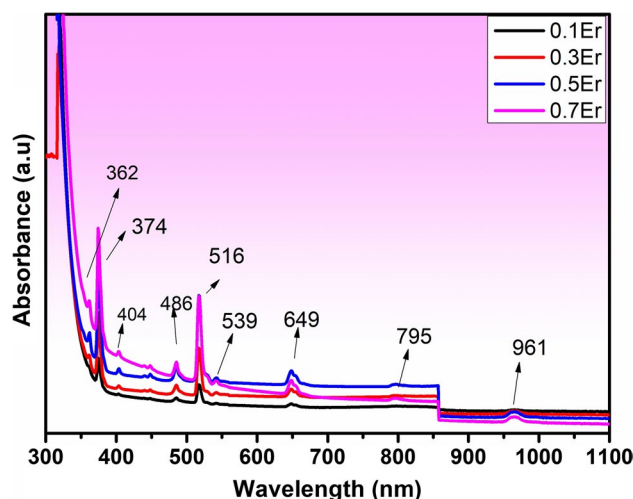


Fig. 2 Optical absorption spectra of Er_2O_3 -doped $(48-x)AlPO_4 + 15 K_2O + 12MgF + 20Na_2O + 5NaF + xEr_2O_3$ glasses

quantity realized in Fig. 1 is corresponds noticeable change in NBOs content formed in the glass structure to allow Er^{3+} ions to enter the glass host [26].

The experimental oscillator strength is the numerical measure of absorption lines of Er^{3+} ions. The value often indicates the strength of electronic transition at wavelength of light absorption [27]. The formula applied the oscillator strength is given by

$$f_{exp} = 4.32 \times 10^{-9} \int \epsilon v \cdot dv \quad (1)$$

where, ϵ denotes the molar extinction coefficient, $v \cdot dv$ is the area under the curve [7, 18]. The density of the glasses, Er^{3+} ion concentration, and thickness of the glass specimens (2 mm) were utilized to compute the molar extinction coefficient.

The calculated values of f_{exp} are tabulated in Table 2. The magnitudes were proportional to the areas under the absorption lines and changed according to the strength of electronic transitions. Among the transitions, the $^4I_{15/2}$ to $^2H_{11/2}$ band's oscillator strength was highest and next highest was for $^4I_{15/2} \rightarrow ^4I_{13/2}$ hypersensitive electronic transition [19]. Nonetheless, f_{exp} value of $^4I_{15/2} \rightarrow ^4F_{7/2}$ was moderate and 977 nm could be considered for one of the potential excitations for suitable emission at NIR and visible emission. According to the spectrum and f_{exp} values wavelength of 380 nm and 980 nm used as excitation wavelength for emission study.

Often the Judd–Ofelt (JO) theory has been employed to understand the influence of structural properties of the glass network on the Er^{3+} ions and ions ability of emission in the glass host [27]. The magnitude of the JO intensity parameter Ω_2 is often correlated with a site-to-site asymmetry

Table 2 Judd–Ofelt parameters Ω_2 , Ω_4 & Ω_6 ($\times 10^{-20}$) and spectroscopic quality values of $(48-x)\text{AlPO}_4 + 15\text{K}_2\text{O} + 12\text{MgF} + 20\text{Na}_2\text{O} + 5\text{NaF} + x\text{Er}_2\text{O}_3$ glasses

Transition (From $^4\text{I}_{15/2}$ ground state)	Energy (cm^{-1})	0.1 Er		0.3 Er		0.5 Er		0.7 Er	
		f_{exp}	f_{cal}	f_{exp}	f_{cal}	f_{exp}	f_{cal}	f_{exp}	f_{cal}
$^4\text{G}_{11/2}$	26,736	5.41	5.62	6.01	6.15	6.54	6.27	3.83	3.82
$(^2\text{G}, ^4\text{F}, ^2\text{H})_{9/2}$	24,782	–	–	–	–	0.32	0.33	0.23	0.25
$^4\text{F}_{7/2}$	20,620	0.96	0.87	1.05	0.95	1.16	0.87	0.61	0.68
$^2\text{H}_{11/2}$	19,329	3.36	3.16	3.29	3.20	3.27	3.52	2.13	2.15
$^4\text{F}_{9/2}$	15,440	0.78	0.82	0.76	0.80	0.74	0.79	0.73	0.72
$^4\text{I}_{11/2}$	10,357	0.16	0.28	0.15	0.21	0.26	0.29	0.14	0.20
$^4\text{I}_{13/2}$	6557	0.59	0.58	0.62	0.65	0.56	0.57	0.45	0.43
δ_{rms}		1.93E–07		2.32E–07		2.40E–07		4.79E–07	
Spectroscopic quality factor		0.927		0.640		0.857		1.323	
Ω_2		2.027E–20		2.250E–20		2.324E–20		1.259E–20	
Ω_4		5.405E–21		5.116E–21		5.035E–21		5.615E–21	
Ω_6		5.830E–21		5.74E–21		5.872E–21		4.245E–21	

change around the Er³⁺ sites and magnitude of covalent bond between Er³⁺ to O²⁻ oxygen ligand [28]. The Ω_6 and Ω_4 indicates rigidity and viscosity of the glass structure. In this work, JO intensity parameters were computed utilizing the least square approach by using the JO equations and reduced square matrix elements mentioned in earlier work [29]. The JO intensity parameters of current host glass and with other glass matrices are shown in Table 2. The trend of JO parameter observed to be $\Omega_2 > \Omega_4 > \Omega_6$ and with respect to ion concentration the Ω_2 magnitude is comparable with the other phosphate and phosphotellurite glass matrices [14, 30, 31]. This change can be attributed to the increase in the site asymmetry nearby the Er³⁺ ions. The decrease of Ω_2 with respect to the ion concentration's can be ascribed to the creation of NBOs [31]. The diminution of Ω_4 value indicates the abatement of glass rigidity around the Er³⁺ ions in the glass matrix. A vital metric for evaluating the radiative transition over non-radiative relaxation of Er³⁺ ions in the glass structure is the spectroscopic quality factor and was calculated by Ω_4/Ω_6 [30]. The quality factor for the 0.5 Er glass listed in Table 2 to be 0.81, which is high compared to other phosphate glass and among other prepared glass specimens utilized in the current study, this illustrate that the stimulated emission can be dominated over non-radiative emission of Er³⁺ ions.

3.4 Excitation and emission properties

The photoluminescence ability of Er³⁺ doped glasses made the revolution in the telecommunication industry as Er³⁺ doped fibre amplifier. The stoke and anti-stoke shift is viable in the case of emission after suitable excitation. In addition, for wavelength down-converting or upconverting applications, the imprint of excitation spectra is necessary. The

Fig. 3 (left) displays the excitation spectra of 1 mol% Er³⁺ loaded glass. The spectra covered the UV to visible region (350–550 nm) and several excitation bands were appeared in the spectrum. The band assignment of appeared peaks were $^4\text{I}_{15/2} \rightarrow ^4\text{G}_{9/2}$ (364.98 nm), $^4\text{I}_{15/2} \rightarrow ^4\text{G}_{11/2}$ (377 nm), $^4\text{I}_{15/2} \rightarrow ^4\text{F}_{9/2}$ at (406 nm), $^4\text{I}_{15/2} \rightarrow ^4\text{F}_{3/2}$ (443 nm), $^4\text{I}_{15/2} \rightarrow ^4\text{F}_{5/2}$ (450 nm) $^4\text{I}_{15/2} \rightarrow ^4\text{F}_{7/2}$ (487 nm) [31]. The excitation wavelengths (λ_{exc}) of 380 and 980 nm were used to excite the glasses for recording the NIR and visible down-conversion and up-conversion emission spectra of glasses used in this study.

The NIR emission spectral results of studied glass hosts were captured under the excitation of 980 nm and presented in the Fig. 3 (right). From the emission spectra presented in Fig. 3 (right), it can be noticed that the intensity of Er³⁺ ions luminous emission of $^4\text{I}_{13/2} \rightarrow ^4\text{I}_{15/2}$ transition changed relatively according to the ion concentration in the glass host. The intensity was highest for 0.5 mol% of Er³⁺ loaded glass and beyond that the decrease in intensity of emission was observed. The high ion concentration in the glass host was led to the Er³⁺ ion clustering and perhaps led to the concentration quenching of emission intensity [31]. However, with respect to the ion concentration in the alumino-phosphate glass, full width half maxima of the overall emission band have been considered and tune in the FWHM of the same band is visible in the spectra. Emission intensity for the 0.5 mol% was optimum and FWHM (96.94 nm) was highest compared to other phosphate glasses [14, 30, 31]. Moreover, bandwidth which is influenced by the FWHM is expected to increase in 0.5 Er glass and thereby help in add in multiplexing channels for light transmission.

The Er³⁺ ions usually exhibit a non-linear emission mechanism at 980 nm excitation. The up-conversion emission curve of the glass has been presented in the Fig. 4

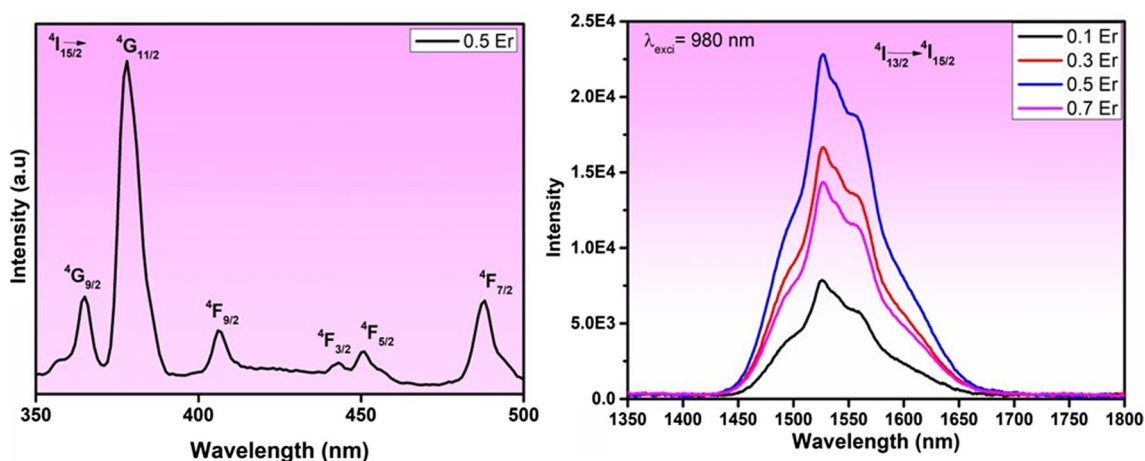


Fig. 3 Excitation (left) and NIR emission (right) spectra of Er^{3+} doped $48\text{AlPO}_4 + 15\text{K}_2\text{O} + 12\text{MgF} + 20\text{Na}_2\text{O} + 5\text{NaF}$ glasses

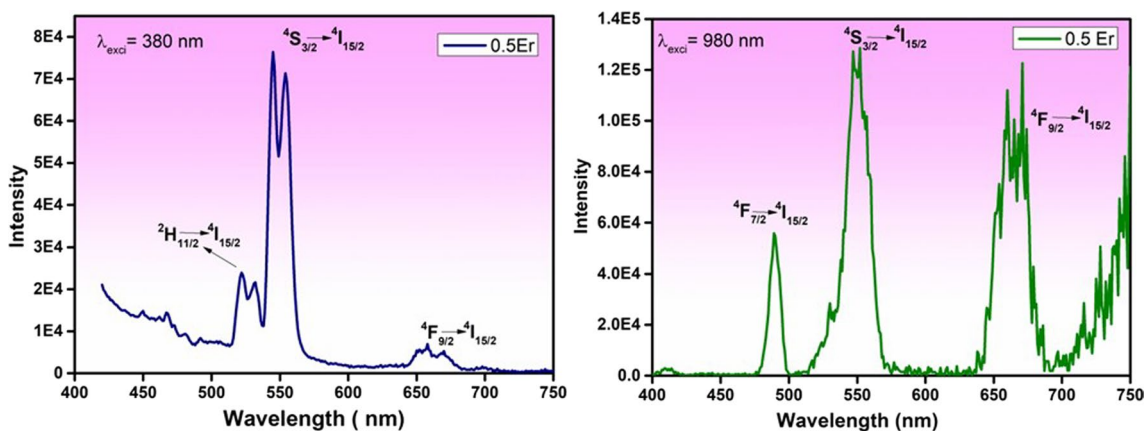


Fig. 4 Emission spectra of Er^{3+} doped $48\text{AlPO}_4 + 15\text{K}_2\text{O} + 12\text{MgF} + 20\text{Na}_2\text{O} + 5\text{NaF}$ glasses at excitation of 380 nm (left) and at the pumping of 980 nm (right)

(left). The optimum 0.5 Er glass shown visible emission curves in the red, green and blue province of the electromagnetic spectrum upon NIR light excitation. The reason for the emission bands lies in electronic transition of ${}^4\text{F}_{9/2} \rightarrow {}^4\text{I}_{15/2}$, ${}^4\text{S}_{3/2} \rightarrow {}^4\text{I}_{15/2}$ and ${}^4\text{F}_{7/2} \rightarrow {}^4\text{I}_{15/2}$ at 664 nm, 550 nm and 488 nm [16]. The intensity of the emission curve in blue is moderate and considerably high for green and after red emission curves. Hence, the Fig. 4 (right) shows, emission spectrum of the same glass at 380 nm excitation. The nature of the luminous emission of Er^{3+} ion differs compared to previous spectrum and it also consists of three emission curves at 658 nm, 554 nm and 521 nm because of electronic transitions of ${}^4\text{F}_{9/2} \rightarrow {}^4\text{I}_{15/2}$, ${}^4\text{S}_{3/2} \rightarrow {}^4\text{I}_{15/2}$ and ${}^2\text{H}_{11/2} \rightarrow {}^4\text{I}_{15/2}$ [32]. The intensity of the luminous band at 554 nm peaked highest and intensity of ${}^4\text{F}_{9/2} \rightarrow {}^4\text{I}_{15/2}$ transition at 658 nm was low. The reason for change in emission of rate of electronic transition is solely attributed to the Er^{3+} excitation mechanism.

Further, the energy scheme diagram of Er^{3+} ion has been used to explain the change in emission profiles of the spectrum at different excitations. Fig. 5 depicts the energy scheme diagram which consist of ground state and other excited states. At 980 nm, the Er^{3+} ions excited from ground state ${}^4\text{I}_{15/2} \rightarrow {}^4\text{I}_{11/2}$ due to ground state absorption (GSA). After that, a few ions are allowed to relax to nearby state ${}^4\text{I}_{13/2}$ and then remaining ions at ${}^4\text{I}_{11/2}$ undergoes excited state absorption (${}^4\text{I}_{11/2} + \text{photon} = {}^4\text{F}_{7/2}$) or energy transfer up-conversion ($({}^4\text{I}_{11/2}, {}^4\text{I}_{11/2}) \rightarrow ({}^4\text{F}_{7/2}, {}^4\text{I}_{15/2})$) to reach ${}^4\text{F}_{7/2}$ state [33, 34]. Then, a significant number of excited ions are relaxed to ground state (${}^4\text{F}_{7/2} \rightarrow {}^4\text{I}_{15/2}$) and resulted in 488 nm photon emission in the spectrum. The large number of ions non-radiatively decays to adjacent levels of ${}^4\text{S}_{3/2}$ and ${}^4\text{F}_{9/2}$ and after ions made transition of ${}^4\text{S}_{3/2} \rightarrow {}^4\text{I}_{15/2}$ by emitting photon of 550 nm and ${}^4\text{F}_{9/2} \rightarrow {}^4\text{I}_{15/2}$ transition resulted in photon of 664 nm wavelength [33]. Moreover, ion transition from ${}^4\text{I}_{13/2} \rightarrow {}^4\text{I}_{15/2}$ resulted in 1532 nm broad band emission.

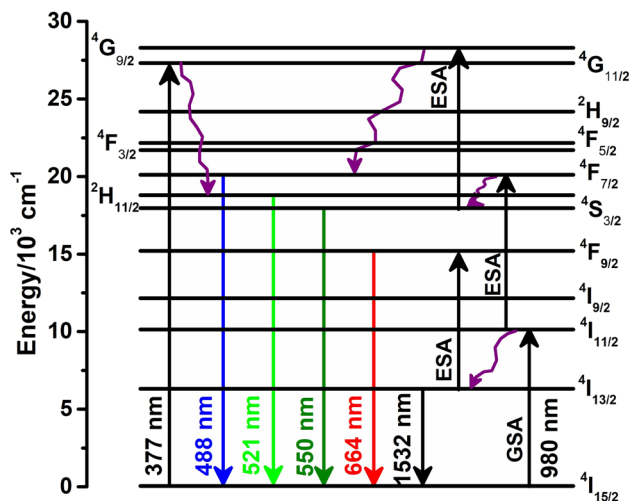


Fig. 5 Schematic energy level diagram of Er³⁺ ion

Interestingly, when glass specimens are excited with 380 nm different emission profiles have been detected. The Er³⁺ ion directly excited to ⁴G_{9/2} state from ground state ⁴I_{15/2} because of UV photon absorption. The excited Er³⁺ ions can be non-radiatively decayed to ⁴F_{9/2}, ⁴S_{3/2} and ²H_{11/2} state and most favourable state for ions accompany is ⁴S_{3/2} according to the selection rule. Further ions are radiatively made transition to ground state by emitting feeble emission at 521 nm, 658 nm and intense emission only at 554 nm. The emission intensity at UV excitation is one order less than NIR photon excitation. This change may be owing to the large absorption cross-section of Er³⁺ content at around 980 nm.

The lifetime of the metastable state of ⁴I_{13/2} was determined after exciting the sample at 980 nm. The relaxation time for photon counting is taken in microsecond regime

and Fig. 6 (left) presents the decay curves of the Er³⁺ loaded glass specimens. In current study, the lifetime was measured after fitting the data to the exponential decay-1 function using Origin software and value was around 0.303 ms. The value of lifetime was found to decrease against the doping concentration on account of increase in non-radiative transition of Er³⁺ ions of 0.5 mol% of Er³⁺ doping into the host glass. The escalation in Er³⁺ ion content in the host glass led to the ion-ion interaction owing to the lessening in inter-ionic distance of Er³⁺ ions in phosphate glass structure [28]. Therefore, only 0.5 Er glass was considered for further evaluation of stimulated emission cross-section and optical gain evaluation and the evaluated values given in Table 3. The results were compared to PBaLaEr: 47.5P₂O₅ + 47.5BaO + 4.5La₂O₃ + 0.5Er₂O₃ [35], S1: 49B₂O₃ + 10BaO + 10ZnO + 10LiF + 10Li₂O + 1Er₂O₃ [36], TZN4: 70TeO₂-20ZnO-6Nb₂O₃ + 4Er₂O₃ [37], ZBaOEr: 69P₂O₅-10Gd₂O₃-10BaO-10ZnO-1Er₂O₃ [38], LBABEr: 20Li₂CO₃-7.5B₂O₃-7.5Al₂O₃-45H₃BO₃-20SiO₂ [39] other phosphate, tellurite and borate glasses. The stimulated emission cross-section (1.30×10^{-20} cm²) and optical gain result of 0.5 Er glass is (0.394×10^{-23} (cm².s)) promising for light amplification and continuous laser applications at 1532 nm.

The 1931 CIE theory has been implemented to understand the aggregate emission colour of the glass due to different emission profiles [18]. The resulted colour chromaticity co-ordinates are indexed in Fig. 6 (right). The luminous colour of the glass changed according to the excitation wavelength and emission colour of the glass was green at 380 nm excitation and it turned into yellowish green when samples are excited with 980 nm. This tune in emission colour is highly useful in the anticounterfeiting and solid-state light emitting devices.

The potential of the glass composition to use as optical amplifier can be evaluated using McCumber (MC) theory.

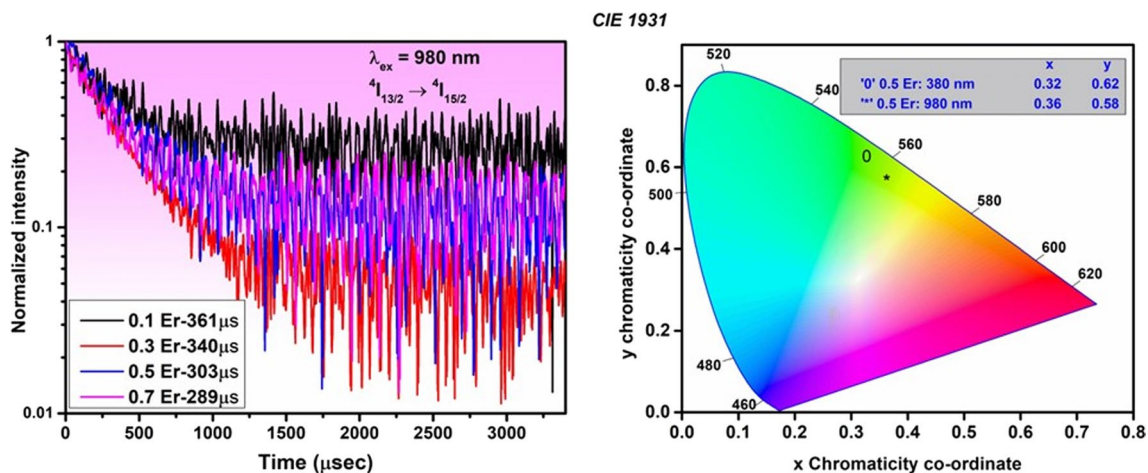


Fig. 6 Decay profile (left) and 1931 CIE chromaticity diagram of Er³⁺ doped 48AlPO₄ + 15 K₂O + 12 MgF + 20 Na₂O + 5NaF glasses

Table 3 Full width half maxima ($\Delta\lambda_p$), total transition probability (A), measured lifetime (τ_{meas}), stimulated emission cross-section (σ_s), gain bandwidth ($\sigma_s \times \Delta\lambda_p$) and optical gain ($\sigma_s \times \tau_{meas}$) of ${}^4I_{13/2} \rightarrow {}^4I_{15/2}$ of 0.5 Er doped 48AlPO₄+15 K₂O+12 MgF+20 Na₂O+5NaF glasses and other glasses studied in recent past

Parameters	0.5 Er	PBaLaEr1	S1	TZN4	ZBaOEr	LBABEr
λ_p (nm)	1526	1530	1531	1530	1535	1538
$\Delta\lambda_p$ (nm)	96.94	59	74	97.8	51	49.2
A (s ⁻¹)	427	270	206	–	–	745
τ_{meas} (ms)	0.303	1.53	3.60	1.93	3.3	0.07
β	1	1	1	–	1	1
Stimulated emission cross section σ_s ($\times 10^{-20}$ cm ²)	1.30	1.35	0.72	0.71	0.44	2.07
Gain bandwidth $\sigma_s \times \Delta\lambda_p$ ($\times 10^{-25}$ cm ³)	1.26	0.8	0.53	–	0.24	1.02
Optical gain $\sigma_s \times \tau_{meas}$ ($\times 10^{-23}$ cm ² .s)	0.394	2.06	3.5	–	–	2.78

For that, essential parameter such as absorption ($\sigma_{abs}(v)$) and emission cross-section ($\sigma_{emi}(v)$) from 1400 to 1600 nm for ${}^4I_{13/2}$ to ${}^4I_{15/2}$ transition of 0.5 Er glass was assessed utilizing the following relation [40, 41],

$$\sigma_{abs}(v) = \frac{2.303}{Nt} A(v) \tag{2}$$

where $A(v)$ is the 0.5Er glass absorbance, t is the thickness of 0.5Er glass and N is related to the concentration of Er³⁺ ion [41]. The change in ($\sigma_{abs}(v)$) with NIR wavelength is plotted and the plot is shown Fig. 7 (left). For 0.5Er emission cross-section,

$$\sigma_{emi}(v) = \sigma_{abs}(v) \exp\left(\frac{\epsilon - hv}{kT}\right) \tag{3}$$

where ϵ is the excitation energy for ${}^4I_{15/2}$ to ${}^4I_{13/2}$ transition of Er³⁺ ion [32] and value gathered for present analysis is 6540 cm⁻¹, hv is the energy attributed to the 0.5 Er glass's NIR emission. The values of $\sigma_{emi}(v)$ with wavelength is plotted in the Fig. 7 (left). The maximum magnitude of $\sigma_{abs}(v)$ and $\sigma_{emi}(v)$ around 1531 nm is found to be 1.30×10^{-20} cm² and it is comparable to other glass matrices [31]. The Fig. 7 (left) indicates overlap in the emission and absorption curve,

which indicates the efficiency of self-absorption at this wavelength. Thus 0.5 Er glass can be matched to broadband optical amplifier applications.

Er³⁺ glass is predicted to be employed as an optical amplifier in communication materials due to its broad and flat gain spectrum, which spans numerous communications windows. The $\sigma_{abs}(v)$ and $\sigma_{emi}(v)$ can be utilized to determine the gain coefficient $G(v)$ as [7].

$$G(v) = \gamma \sigma_{emi}(v) - (1 - \gamma) \sigma_{abs}(v) \tag{4}$$

where γ (0–1, in increment) is shows the population inversion. The terminology of parameter γ is stated explicitly as the ratio of the quantity of Er³⁺ ions in the metastable level to the quantity of Er³⁺ ions in the lower ground levels. The gain coefficient variation of 0.5 Er glass with wavelength is shown in Fig. 7 (right). The flat gain curve covered the L, C, S and E bands. As the population in an excited level increased, the gain coefficient also increased. In this study, gain coefficient turned into positive after $\gamma = 0.5$, thus population inversion is more than 50% and lasing action is easily achievable around 1531 nm [7]. According to the flat gain curve, L and E windows between 1530 and 1565 nm (C band) and 1460 and 1530 nm (S band), the glass specimens

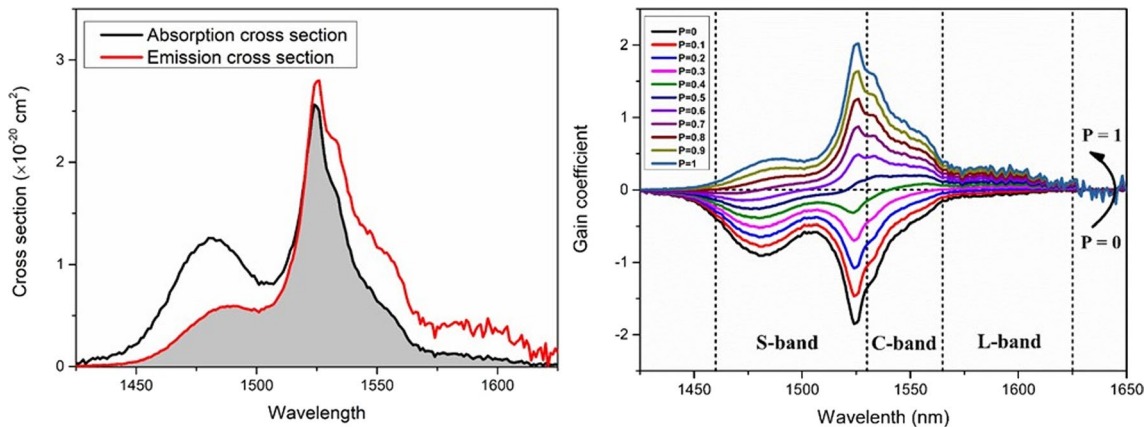


Fig. 7 Cross-section overlay (left) and gain coefficient curve (right) of 0.5 mol% of Er³⁺ doped 48AlPO₄+15 K₂O+12 MgF+20 Na₂O+5NaF glasses

showed a promising gain response for optical amplification purposes in C + S communication window.

4 Summary

The Er³⁺ doped (48-x)AlPO₄ + 15K₂O + 12MgF + 20Na₂O + 5NaF + xEr₂O₃ glass matrix was prepared utilizing melt quench process. The refractive index and density of the glass specimens were increased and inter-atomic distance decreased with the Er³⁺ ion doping into the glass structure. The XRD profile of the glass was broad and diffused due to amorphous structure of the glass. The FTIR vibrational spectra of the glass confirmed the Q⁽¹⁾ (pyrophosphate), Q⁽⁰⁾ (orthophosphate tetrahedra) and Q⁽²⁾ (metaphosphate) units in the glass network. Using absorption intensity values of the glasses JO parameters were determined and trend ($\Omega_2 > \Omega_4 > \Omega_6$) of the JO parameter indicated the strong covalent bond between the oxygen ligand and Er³⁺ ions. The NIR emission profiles of the glass was broaden and intensity was highest for 0.5 Er glass. The metastable ⁴I_{13/2} state lifetime of the excited ion after 980 nm excitation is 0.3 ms in 0.5 Er glass and optical gain offered by the same glass is 0.394 × 10⁻²³ cm²s. The two photon up-conversion of Er³⁺ ions at 0.5 Er glass resulted blue, green and red color emission in the spectrum and the emission colour of the glass was yellowish green. However, the down-conversion emission spectra of 0.5 Er glass was dominated by green light emission. The change in emission colour of the glass is more affable for solid state lighting applications. Large bandwidth, experimental lifetime, stimulated emission cross-section and optical gain values of 0.5 Er glass suits for C and L band light production and amplification applications.

Acknowledgements The authors express their gratitude to Princess Nourah bint Abdulrahman University Researchers Supporting Project number (PNURSP2024R2), Princess Nourah bint Abdulrahman University, Riyadh, Saudi Arabia. R. Rajaramakrishna would like to thank for the kind support for the research through the Strategic Academic Leadership Program “Priority-2030”, Siberian Federal University, Krasnoyarsk, Russia.

Author contributions VH: Conceptualization, Methodology, Data Curation, Writing–Original Draft and Editing, Writing–Review, KRV: Data Curation, SDK: Conceptualization, Methodology, Writing–Review and Editing, Project administration, CSDV: Data curation, Software, AHA: Data curation, Writing–Review and Editing, MIS: Methodology, Data Curation, Writing–Review and Editing, GJ: Methodology, Data Curation, Formal analysis, Writing–Original Draft and Editing, Writing–Review and Editing, RR: Formal analysis, Software, Writing–Review, KK: Methodology, Data Curation, Formal analysis, Writing–Review.

Funding The authors express their gratitude to Princess Nourah bint Abdulrahman University Researchers Supporting Project number (PNURSP2024R2), Princess Nourah bint Abdulrahman University, Riyadh, Saudi Arabia.

Data availability The raw data that support the findings are available on request from the corresponding author.

Declarations

Conflict of interest The authors declare no conflict of interest.

References

1. P. Babu, H.J. Seo, C.R. Kesavulu, K.H. Jang, C.K. Jayasankar, Thermal and optical properties of Er³⁺-doped oxyfluorotellurite glasses. *J. Lumin.* **129**, 444–448 (2009). <https://doi.org/10.1016/j.jlumin.2008.11.014>
2. A. Jha, B. Richards, G. Jose, T. Teddy-Fernandez, P. Joshi, X. Jiang, J. Lousteau, Rare-earth ion doped TeO₂ and GeO₂ glasses as laser materials. *Prog. Mater. Sci.* **57**, 1426–1491 (2012). <https://doi.org/10.1016/j.pmatsci.2012.04.003>
3. C. Madhukar Reddy, B. Deva Prasad Raju, N. John Sushma, N.S. Dhoble, S.J. Dhoble, A review on optical and photoluminescence studies of RE³⁺ (RE=Sm, Dy, Eu, Tb and Nd) ions doped LCZSFB glasses. *Renew. Sustain. Energy Rev.* **51**, 566–584 (2015). <https://doi.org/10.1016/j.rser.2015.06.025>
4. C. Wang, M. Zhang, Y. Chen, Y. Wang, J. Lu, X. Huang, Y. Wei, L. Wan, S. Huang, Z. Li, Z. Chen, Z. Li, Synthesis and study of novel erbium-doped La₂O₃-Al₂O₃ glasses for on-chip waveguide amplifier. *J. Alloys Compd.* **899**, 162915 (2022). <https://doi.org/10.1016/j.jallcom.2021.162915>
5. F. Lahoz, C. Pérez-Rodríguez, S.E. Hernández, I.R. Martín, V. Lavín, U.R. Rodríguez-Mendoza, Upconversion mechanisms in rare-earth doped glasses to improve the efficiency of silicon solar cells. *Sol. Energy Mater. Sol. Cells* **95**, 1671–1677 (2011). <https://doi.org/10.1016/j.solmat.2011.01.027>
6. A. Lemiere, B. Bondzior, I. Aromäki, L. Petit, Study of visible, NIR, and MIR spectroscopic properties of Er³⁺-doped tellurite glasses and glass–ceramics. *J. Am. Ceram. Soc.* **105**, 7186–7195 (2022). <https://doi.org/10.1111/jace.18649>
7. C.R. Kesavulu, H.J. Kim, S.W. Lee, J. Kaewkhao, N. Wantana, S. Kothan, S. Kaewjaeng, Influence of Er³⁺ ion concentration on optical and photoluminescence properties of Er³⁺-doped gadolinium–calcium silica borate glasses. *J. Alloys Compd.* **683**, 590–598 (2016). <https://doi.org/10.1016/j.jallcom.2016.04.314>
8. X. Huang, H. Cheng, W. Luo, W. Zhang, M. Jiang, C. Yang, T. Yu, Z. Cai, Z. Xu, X. Shu, Z. Yang, J. Qiu, S. Zhou, Er-activated hybridized glass fiber for laser and sensor in the extended wavebands. *Adv. Opt. Mater.* **9**, 2101394 (2021). <https://doi.org/10.1002/adom.202101394>
9. X. Feng, S. Tanabe, T. Hanada, Spectroscopic properties and thermal stability of Er³⁺-doped germanotellurite glasses for broadband fiber amplifiers. *J. Am. Ceram. Soc.* **84**, 165–171 (2001). <https://doi.org/10.1111/j.1151-2916.2001.tb00625.x>
10. X. Shen, S. Chen, Y. Sun, X. Wang, W. Wei, L. Hu, Investigation of Er³⁺-doped phosphate glass for L+ band optical amplification. *IEEE Photonics J.* **13**, 2200506 (2021). <https://doi.org/10.1109/JPHOT.2021.3124132>
11. H.C. Çamiçi, T. Guérineau, V.A.G. Rivera, R.F. Falci, S. LaRochelle, Y. Messaddeq, The role of tungsten oxide in Er³⁺-doped bismuth-germanate glasses for optical amplification in L-band. *Sci. Rep.* **13**, 8835 (2023). <https://doi.org/10.1038/s41598-023-35995-8>
12. P. Joshi, S. Shen, A. Jha, Er³⁺-doped boro-tellurite glass for optical amplification in the 1530–1580nm. *J. Appl. Phys.* (2008). <https://doi.org/10.1063/1.2908873>

13. D. Pugliese, A. Veber, A. Lemièrre, N.G. Boetti, L. Petit, Effect of post-heat-treatment on the structural, spectroscopic and dissolution properties of a highly stable Er³⁺-doped multi-component phosphate glass. *J. Alloys Compd.* **883**, 160878 (2021). <https://doi.org/10.1016/j.jallcom.2021.160878>
14. F. Zaman, G. Rooh, N. Chanthima, S.U. Khan, H.J. Kim, S. Kothan, N. Chanlek, M. Arshad, J. Kaewkhao, Investigation of spectroscopic and photoluminescence properties of Erbium doped phosphate (P₂O₅-K₂O₃-Al₂O₃) glasses. *J. Alloys Compd.* **893**, 162215 (2022). <https://doi.org/10.1016/j.jallcom.2021.162215>
15. L.R. Moorthy, M. Jayasimhadri, S.A. Saleem, D.V.R. Murthy, Optical properties of Er³⁺-doped alkali fluorophosphate glasses. *J. Non Cryst. Solids* **353**, 1392–1396 (2007). <https://doi.org/10.1016/j.jnoncrysol.2006.10.062>
16. B. Afef, M.M. Alqahtani, H.H. Hegazy, E. Yousef, K. Damak, R. Maâlej, Green and near infrared emission of Er³⁺ doped PZS and PZC glasses. *J. Lumin.* **194**, 706–712 (2018). <https://doi.org/10.1016/j.jlumin.2017.09.040>
17. N. Deopa, M.K. Sahu, S. Kaur, A. Prasad, K. Swapna, V. Kumar, R. Punia, A.S. Rao, Enhanced visible green and 1.5 μm radiative emission of Er³⁺ ions in Li₂O-PbO-Al₂O₃-B₂O₃ glasses for photonic applications. *J. Rare Earths* **39**, 520–525 (2021). <https://doi.org/10.1016/j.jre.2020.05.002>
18. V. Hegde, C.S.D. Viswanath, V. Upadhyaya, K.K. Mahato, S.D. Kamath, Red light emission from europium doped zinc sodium bismuth borate glasses. *Physica B Condens. Matter* **527**, 35–43 (2017). <https://doi.org/10.1016/j.physb.2017.09.113>
19. P. Ramprasad, Ch. Basavapoornima, C.R. Kesavulu, V. Venkatramu, J. Kaewkhao, C.K. Jayasankar, Spectroscopic properties of Er³⁺-doped barium phosphate glasses for optical gain media. *Results Opt.* **12**, 100489 (2023). <https://doi.org/10.1016/j.rio.2023.100489>
20. M. Lu, F. Wang, Q. Liao, K. Chen, J. Qin, S. Pan, FTIR spectra and thermal properties of TiO₂-doped iron phosphate glasses. *J. Mol. Struct.* **1081**, 187–192 (2015). <https://doi.org/10.1016/j.molstruc.2014.10.029>
21. A.H. Almuqrin, M. Rashad, C.V. More, M.I. Sayyed, M. Elsafi, An experimental and theoretical study to evaluate Al₂O₃-PbO-B₂O₃-SiO₂-BaO radiation shielding properties. *Rad. Phys. Chem.* **222**, 111824 (2024). <https://doi.org/10.1016/j.radphyschem.2024.111824>
22. Y.B. Saddeek, M.A. Kaid, M.R. Ebeid, FTIR and physical features of Al₂O₃-La₂O₃-P₂O₅-PbO glasses. *J. Non Cryst. Solids* **387**, 30–35 (2014). <https://doi.org/10.1016/j.jnoncrysol.2013.12.029>
23. Z.A.S. Mahraz, E.S. Sazali, M.R. Sahar, N.U. Amran, S.N.S. Yaacob, S.M. Aziz, S.Q. Mawlood, F.M. Noor, A.N. Harun, Spectroscopic investigations of near-infrared emission from Nd³⁺-doped zinc-phosphate glasses: Judd-Ofelt evaluation. *J. Non Cryst. Solids* **509**, 106–114 (2019). <https://doi.org/10.1016/j.jnoncrysol.2018.05.013>
24. H.J. Alasali, U. Rilwan, K.A. Mahmoud, T.A. Hanafy, M.I. Sayyed, Comparative analysis of TiO₂, Fe₂O₃, CaO and CuO in borate based glasses for gamma ray shielding. *Nucl. Engg. Technol.* **56**, 1845 (2024). <https://doi.org/10.1016/j.net.2023.12.042>
25. P.K. Jha, O.P. Pandey, K. Singh, Structure and crystallization kinetics of Li₂O modified sodium-phosphate glasses. *J. Mol. Struct.* **1094**, 174–182 (2015). <https://doi.org/10.1016/j.molstruc.2015.03.066>
26. A. Kaur, A. Khanna, L.I. Aleksandrov, Structural, thermal, optical and photo-luminescent properties of barium tellurite glasses doped with rare-earth ions. *J. Non Cryst. Solids* **476**, 67–74 (2017). <https://doi.org/10.1016/j.jnoncrysol.2017.09.025>
27. S. Tanabe, T. Ohyagi, N. Soga, T. Hanada, Compositional dependence of Judd-Ofelt parameters of Er ions in alkali-metal borate glasses. *Phys. Rev. B* **46**, 3305–3310 (1992). <https://doi.org/10.1103/PhysRevB.46.3305>
28. Sk.N. Rasool, B.C. Jamalalaih, K. Suresh, L.R. Moorthy, C.K. Jayasankar, Spectroscopic properties of Er³⁺-doped phosphate based glasses for broadband 1.54 μm emission. *J. Mol. Struct.* **1130**, 837–843 (2017). <https://doi.org/10.1016/j.molstruc.2016.10.090>
29. W.T. Carnall, P.R. Fields, K. Rajnak, Electronic energy levels in the trivalent lanthanide aquo ions. I. Pr³⁺, Nd³⁺, Pm³⁺, Sm³⁺, Dy³⁺, Ho³⁺, Er³⁺, and Tm³⁺. *J. Chem. Phys.* **49**, 4424–4442 (1968). <https://doi.org/10.1063/1.1669893>
30. A. Amarnath Reddy, S. Surendra Babu, G. Vijaya Prakash, Er³⁺-doped phosphate glasses with improved gain characteristics for broadband optical amplifiers. *Opt. Commun.* **285**, 5364–5367 (2012). <https://doi.org/10.1016/j.optcom.2012.08.031>
31. K. Selvaraju, K. Marimuthu, Structural and spectroscopic studies on concentration dependent Er³⁺ doped boro-tellurite glasses. *J. Lumin.* **132**, 1171–1178 (2012). <https://doi.org/10.1016/j.jlumin.2011.12.056>
32. G. Devarajulu, G. Lakshminarayana, P. Venkateswara-Rao, D.-E. Lee, J. Yoon, T. Park, Er³⁺-doped SiO₂-based glasses: an exploration of structural, visible, chromatic, and NIR fluorescence characteristics. *Mater. Res. Bull.* **147**, 111634 (2022). <https://doi.org/10.1016/j.materresbull.2021.111634>
33. C. Basavapoornima, K. Linganna, C.R. Kesavulu, S. Ju, B.H. Kim, W.T. Han, C.K. Jayasankar, Spectroscopic and pump power dependent upconversion studies of Er³⁺-doped lead phosphate glasses for photonic applications. *J. Alloys Compd.* **699**, 959–968 (2017). <https://doi.org/10.1016/j.jallcom.2016.12.199>
34. M.E. Alvarez-Ramos, F. Félix-Domínguez, G. Saavedra-Rodríguez, R.C. Carrillo-Torres, Structural, luminescent and upconversion characteristics of Er³⁺ doped titanium zinc tellurite glass. *Opt. Mater.* **120**, 111413 (2021). <https://doi.org/10.1016/j.optmat.2021.111413>
35. B.N. Swetha, G. Devarajulu, K. Keshavamurthy, G. Jagannath, H.R. Deepa, Enhanced 1.53 μm emission of Er³⁺ in nano-Ag embedded sodium-boro-lanthanate glasses. *J. Alloys Compd.* **856**, 158212 (2021). <https://doi.org/10.1016/j.jallcom.2020.158212>
36. G. Lakshminarayana, A.N. Meza-Rocha, O. Soriano-Romero, U. Caldiño, A. Lira, D.E. Lee, J. Yoon, T. Park, Assessment of optical and fluorescence aspects of Er³⁺-doped multicomponent B₂O₃ glasses as active media for 1.532 μm near-infrared optical amplifiers. *J. Mater. Res. Technol.* **18**, 3457–3477 (2022). <https://doi.org/10.1016/j.jmrt.2022.04.012>
37. F. Aouaini, A. Maaoui, N.B.H. Mohamed, M.M. Alanazi, L.A. El Maati, Visible to infrared down conversion of Er³⁺ doped tellurite glass for luminescent solar converters. *J. Alloys Compd.* (2022). <https://doi.org/10.1016/j.jallcom.2021.162506>
38. M. Shoaib, I. Khan, N. Chanthima, A. Alhuthali, N. Intachai, S. Kothan, A. Ahad, I. Ullah, S. Khattak, G. Rooh, J. Kaewkhao, T. Ahmad, Photoluminescence analysis of Er³⁺-ions doped P₂O₅-Gd₂O₃/GdF₃-BaO-ZnO glass systems. *J. Alloys Compd.* (2022). <https://doi.org/10.1016/j.jallcom.2022.163766>
39. M. Kumar, M.K. Sahu, S. Kaur, A. Prasad, R. Bajaj, R.A. Talewar, Y. Tayal, K. Swapna, A.S. Rao, Visible and NIR spectral analysis of Er³⁺ doped LiBiAlBSi glasses for laser applications. *J. Mater. Sci. Mater. Electron.* (2024). <https://doi.org/10.1007/s10854-024-12281-5>
40. A. Jose, S. Gopi, T. Krishnapriya, T.A. Jose, C. Joseph, N.V. Unnikrishnan, P.R. Biju, Spectroscopic investigations on 1.53 μm NIR emission of Er³⁺ doped multicomponent borosilicate glasses for telecommunication and lasing applications. *Mater. Chem. Phys.* **261**, 124223 (2021). <https://doi.org/10.1016/j.matchemphys.2021.124223>
41. N.S. Prabhu, A.N. Meza-Rocha, O. Soriano-Romero, U. Caldiño, E.F. Huerta, C. Falcony, M.I. Sayyed, H. Al-Ghamdi, A.H. Almuqrin, S.D. Kamath, Spectroscopic study of Er³⁺ doped borate glass system for green emission device NIR laser, and optical

amplifier applications. *J. Lumin.* **238**, 118216 (2021). <https://doi.org/10.1016/j.jlumin.2021.118216>

Publisher's Note Springer Nature remains neutral with regard to jurisdictional claims in published maps and institutional affiliations.

Springer Nature or its licensor (e.g. a society or other partner) holds exclusive rights to this article under a publishing agreement with the author(s) or other rightsholder(s); author self-archiving of the accepted manuscript version of this article is solely governed by the terms of such publishing agreement and applicable law.